

The X-ray afterglow of GRB 020322

D. Watson¹, J. N. Reeves¹, J. P. Osborne¹, J. A. Tedds¹, P. T. O'Brien¹, L. Tomas², and M. Ehle²

¹ X-ray Astronomy Group, Dept. of Physics and Astronomy, University of Leicester, Leicester LE1 7RH, UK

² XMM-Newton Science Operations Centre, European Space Agency, P. O. Box 50727, 28080 Madrid, Spain

Received ; accepted

Abstract. The spectrum of the afterglow of GRB 020322 is the highest-quality X-ray spectrum of a GRB afterglow available to date. It was detected by *XMM-Newton* in an observation starting fifteen hours after the GRB with a mean 0.2–10.0 keV observed flux of $3.5 \pm 0.2 \times 10^{-13}$ erg cm⁻² s⁻¹, making it the brightest X-ray afterglow observed so far with *XMM-Newton*. The source faded; its lightcurve was well fit by a power-law with a decay index of 1.26 ± 0.23 . The spectrum is adequately fit with a power-law absorbed with neutral or ionised gas significantly in excess of the foreground Galactic column, at redshift $1.8_{-1.1}^{+1.0}$ or with low metal abundances. No spectral line or edge features are detected at high significance, in particular, a thermal emission model fits the data poorly, the upper limit on its contribution to the spectrum is 3.7×10^{-14} erg cm⁻² s⁻¹, or $\sim 10\%$ of the total flux. No spectral variability is observed.

Key words. Gamma rays: bursts – X-rays: general

1. Introduction

Gamma-ray burst (GRB) afterglows are most often detected at X-ray energies (Piro 2001), the majority of bursts producing no detectable optical afterglow emission (Fynbo et al. 2001). Most redshift estimates, however, are made from the absorption spectrum of the optical transient or the apparent host galaxy. Recently however, emission lines have been detected in X-ray afterglows, allowing estimates to be made of the cosmological redshifts and the outflow velocities of at least the line-emitting component of the afterglow material (Piro et al. 2000, Reeves et al. 2002b, Watson et al. 2002). In particular, the fact that metal-enriched thermal emission models fit the highest-signal afterglow spectra better than power-law models (Reeves et al. 2002b, Watson et al. 2002) has led to the strengthening of the case for the association of long duration GRBs with the recent collapse of a massive star (Woosley 1993, Vietri & Stella 1998, Lazzati et al. 2001) and to the assertion that thermal emission may be common in GRB afterglows (Watson et al. 2002). *XMM-Newton* (Jansen et al. 2001) has managed relatively rapid responses to GRB alerts (on the order of half a day) and, with its large effective area, has captured the high-quality spectra that have allowed these detections to be made.

Previous detections of emission lines in GRB afterglows with *BeppoSAX*, *ASCA* and *Chandra* have concentrated on emission from highly-ionised iron (Piro et al. 1998, 2000, Antonelli et al. 2000, Yoshida et al. 2001); however the recent observations with *XMM-Newton* have shown emission features

at lower energies (due in part to its very good sensitivity in the soft X-ray band).

In Sect. 2 we report on the observations of the afterglow of GRB 020322, explaining the data reduction procedure in Sect. 3 and presenting the spectrum and lightcurve in Sect. 4. In Sect. 5 the implications of these results are discussed. Conclusions are in Sect. 6. Unless otherwise stated, all errors quoted are 90% confidence limits for one parameter of interest, upper and lower limits are 99.7% (3σ) confidence limits and coordinates are equatorial, J2000.

2. Observations of GRB 020322

GRB 020322 was detected by *BeppoSAX* with the wide field camera (WFC) on 22 March 2002, 03:51:30 UT (Piro 2002) and followed 7.5 hours later with a detection in the MECS instrument (Gandolfi 2002). The position, (MECS: RA = 18h 00m 49.4s, Dec. = +81° 06' 10.8''), was well-determined, with an error-radius of 3' in the WFC and 1.5' in the MECS (see Fig. 1).

XMM-Newton began observing this position at 18:46 UT with EPIC-MOS and 19:17 UT with EPIC-pn, approximately fifteen hours after the burst, Ehle et al. (2002) reporting detection of a bright source with a positional accuracy of $\sim 6''$. A fading optical source was detected within this initial *XMM-Newton* error-circle (Bloom et al. 2002b, Greiner et al. 2002, McMillan et al. 2002) at RA = 18h01m02.98s, Dec. = +81° 06' 28''.17 (Bloom et al. 2002c) with R-band magnitudes of 23.26 ± 0.32 and 23.80 ± 0.30 at 10:39 UT and 23:46 UT respectively, suggesting an early-time power-law decay slope of ~ 0.5 . The field was imaged with the STIS instrument on *HST*

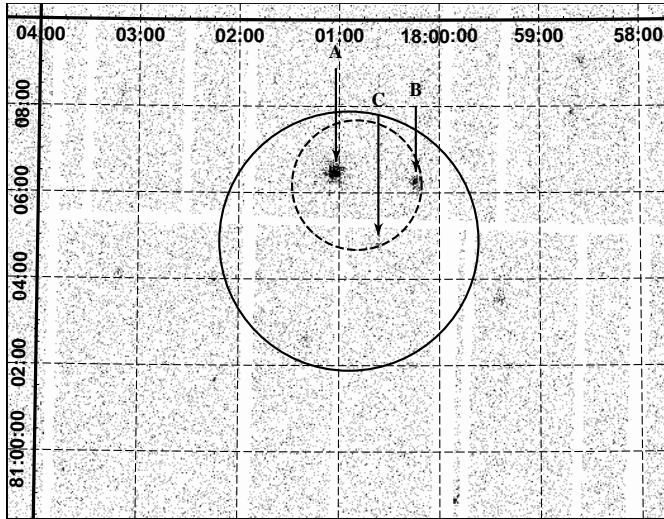


Fig. 1. EPIC-pn 0.2–10 keV-band image of GRB 020322. The *BeppoSAX* WFC (solid circle – 3' radius) and MECS (dashed circle – 1.5' radius) error-circles are shown. Three sources are detected within the MECS error-circle, labelled 'A', 'B' and 'C'; 'A' is the only fading source in the EPIC data and is taken to be the X-ray afterglow of the burst. Coordinate axes plotted are equatorial, R.A. and Dec. (J2000).

on 8 April and 5 May 2002, no optical transient was detected (implying a late-time power-law decay slope steeper than 2.0, Burud et al. 2002), however a galaxy of magnitude ~ 27 was detected at the position of the optical transient, probably the host. No redshift has so far been determined for the GRB or the host galaxy.

3. *XMM-Newton*-EPIC data reduction and analysis

Effective exposure durations were 24 ks and 28 ks for the EPIC-pn (Strüder et al. 2001) and MOS (Turner et al. 2001) cameras respectively, each in full frame mode using the thin filters. The data were processed and reduced with the SAS, version 5.3, datasets from both EPIC-MOS cameras were co-added. MOS and pn spectra were fit individually, yielded consistent results and were therefore fit simultaneously; the lightcurves were compared for each instrument and were, again, consistent and were therefore co-added and fit as a single dataset. Source extraction regions were 40'' in radius and off-source background extraction regions of 80'' radius were chosen. Both single and double pattern (as well as triple and quadruple pattern for the MOS), good (FLAG=0) events were used with response matrices generated for each spectrum. The spectra were binned with a minimum of 20 counts per bin. The final X-ray source positions were determined after cross-correlation with the USNO A2.0 optical catalogue based on the SAS task *eposcorr* (see Tedds & Watson 2002).

Three sources were detected in the *BeppoSAX*-MECS error-circle (Fig. 1). The brightest, with coordinates RA = 18h01m03.1s, Dec. = +81° 06' 27''.9, and a 68% error radius of 0.5'', (source 'A' in Fig. 1) was seen to fade (Fig. 2), with a probability of constancy of 6×10^{-12} . It is interesting to note the very good correspondence ($< 0.5''$ separation) between this source position and that of the optical transient of

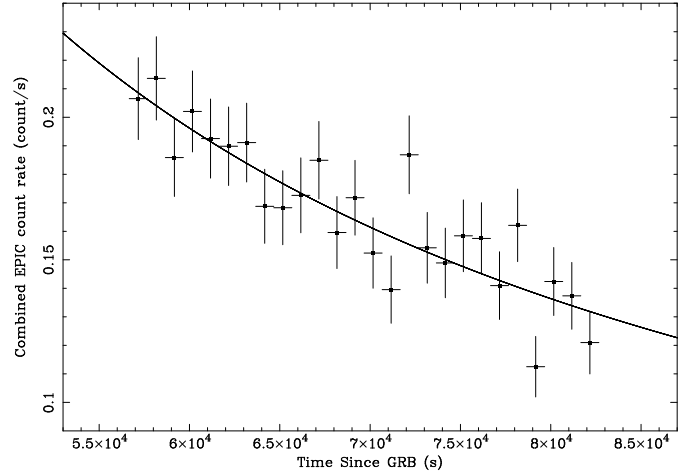


Fig. 2. Combined EPIC-pn and MOS lightcurve of the 0.2–12 keV afterglow of GRB 020322. The best-fit power-law decay ($\chi^2 = 25.2$ for 24 degrees of freedom) is plotted and has a decay index of 1.26 ± 0.23 .

Bloom et al. (2002c), at RA = 18h01m02.98s $\pm 0''.30$, Dec. = +81° 06' 28''.17 $\pm 0''.35$.

A power-law decay ($F \propto t^{-\beta}$) with index $\beta = 1.26 \pm 0.23$ fits the lightcurve well ($\chi^2_{\nu} = 1.05$). We identify this source as the afterglow of GRB 020322. The Galactic hydrogen absorbing column in this direction is $4.6 \times 10^{20} \text{ cm}^{-2}$ (Dickey & Lockman 1990, using the FTOOL *nh*). Its mean observed 0.2–10.0 keV flux was $3.5 \times 10^{-13} \text{ erg cm}^{-2} \text{ s}^{-1}$, making it the brightest GRB afterglow observed by *XMM-Newton* so far, roughly comparable in source counts to the afterglow of GRB 011211 (Reeves et al. 2002b,a). The other sources ('B' and 'C' in Fig. 1) are both on the edge of the MECS error-circle, are fainter ('B' = $6.3 \pm 0.5 \times 10^{-14} \text{ erg cm}^{-2} \text{ s}^{-1}$ and 'C' = $2.5^{+0.3}_{-1.0} \times 10^{-14} \text{ erg cm}^{-2} \text{ s}^{-1}$) and show no evidence for variability (null hypothesis probabilities of 0.95 and 0.69 respectively).

4. Results

The complete EPIC spectrum (Fig. 3) is not well fit with a Galactic-absorbed power-law model, $\chi^2 = 437.4$ for 234 degrees of freedom (DoF). Adding redshifted neutral absorption, the fit becomes acceptable ($\chi^2/\text{DoF} = 241.5/232$), equivalent to a best-fit local excess hydrogen column density of $1.6^{+0.3}_{-0.2} \times 10^{21} \text{ cm}^{-2}$, however there are no significantly detected absorption edges in the spectrum, indicating that the redshift is probably greater than 0.7 (the 90% confidence limit, derived largely from the lack of detection of the neutral Oxygen absorption edge), with a best-fit redshift of $1.8^{+1.0}_{-1.1}$. The best-fit neutral absorbing column density at $z = 1.8$ is $1.3 \pm 0.2 \times 10^{22} \text{ cm}^{-2}$. It is possible that the metal abundance in the absorbing gas is low, which would also explain the lack of absorption edges (this seems unlikely however, given the probability that GRBs occur in star-forming regions, e.g. Holland & Hjorth 1999). At $z = 0$, abundances < 0.4 times the solar values are required to fit the data.

It has been posited that GRBs in dense star-forming regions will photoionise the circumburst medium (Böttcher et al. 1999), giving rise to a NEI plasma. Ionised absorption cannot

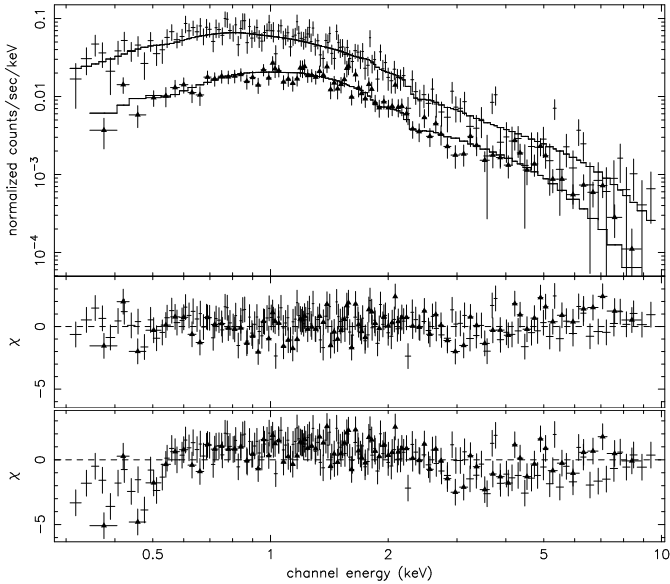


Fig. 3. EPIC-pn (crosses) and combined EPIC-MOS (triangles) spectrum of the afterglow of GRB 020322 fit with a power-law absorbed by the Galactic column ($4.6 \times 10^{20} \text{ cm}^{-2}$) and a redshifted neutral absorber. The residuals to this fit are shown in the middle panel. This model fits the data adequately ($\chi^2_\nu = 1.04$). Residuals to a model fit involving a power-law absorbed only by the Galactic column are plotted in the bottom panel. This model does not fit the data well ($\chi^2_\nu = 1.87$).

be ruled out in this case, with an upper limit of $140 \text{ erg cm s}^{-1}$ to the ionisation parameter of the absorber; a fit where the excess absorption is ionised, with variable iron abundance, gives as good a fit as the neutral absorption case ($\chi^2/\text{DoF} = 239.4/230$). The redshift in the case of the ionised absorber is still constrained, primarily by the Fe-L shell and O VIII-K absorption edges. Fixing the ionisation parameter at the upper limit gives a 90% confidence interval for the redshift of 2.4–2.9. In the case where the absorber is not in equilibrium (see for instance the marginal detection of, and possible explanations for, a transient absorption feature in Amati et al. 2000, Lazzati & Perna 2002), the range of ionization states will be increased, however it is the non-detection of an absorption feature that is the primary lower constraint on the redshift, implying that the redshift limits still hold in the case of a non-equilibrium absorber.

An absorption edge is marginally detected ($\chi^2/\text{DoF} = 233.5/230$, $\geq 98\%$ significance) at 2.8 keV in the observed frame. Attributing this to the K-edge of neutral iron (at 7.1 keV) implies a redshift of 1.6, neutral Co (at 7.7 keV) implies $z = 1.8$, neutral Ni (at 8.3 keV) implies $z = 2.0$; all of which are within the 1σ error bounds of the redshift determination from the fit to the absorption. Allowing the abundance of iron to vary in the model excess absorber however, does not improve the fit significantly.

There is no evidence for any significant detection of emission features in the spectrum. The best-fit parameter values are presented in Table 1.

In order to assess spectral variability, the data were divided in two parts. The data were extracted from the first 11 ks and from the remaining 15 ks in order to have roughly equal numbers of source counts in each spectrum. The start time of the pn

Table 1. Best-fit parameter values fitting a Galactic-absorbed power-law with variable redshifted neutral absorption to a) the complete EPIC dataset, b) the first 11 ks of exposure and c) the remaining 15 ks of exposure. Ninety percent confidence intervals are quoted in parentheses under the relevant value.

	Obs. Flux ($10^{-13} \text{ erg cm}^{-2} \text{ s}^{-1}$)	Γ	z	N_{H} at $z = 0$ (10^{21} cm^{-2})
Complete	3.5 (3.3–3.7)	2.06 (1.98–2.14)	1.8 (0.7–2.8)	1.6 (1.4–1.9)
0–11 ks	3.8 (3.4–4.4)	2.1 (2.0–2.3)	0.20 (0.04–4.1)	1.7 (1.3–2.1)
11–26 ks	3.2 (3.0–3.5)	2.0 (1.9–2.1)	1.7 (0.6–>5)	1.4 (1.1–1.8)

exposure was used as the start time for both the MOS and pn datasets. There is no significant difference between the best-fit parameters for the first and second part spectra (Table 1). The data were also divided into 5 ks parts to assess spectral variability on a shorter time scale; again there is no significant difference between the spectra.

Given the recent results from *XMM-Newton* implying that thermal emission features may be common in early-time X-ray afterglows (Watson et al. 2002), these data were tested to determine limits on thermal emission with the plasma model used in Reeves et al. (2002b) and Watson et al. (2002). The addition of a collisionally-ionised plasma model (the ‘mekal’ model, Mewe et al. 1985, Liedahl et al. 1995) to the absorbed power-law model does not improve the fit significantly, ($\chi^2/\text{DoF} = 239.1/229$, giving an f -test probability for the addition of three extra terms of 0.49) and yields significantly worse fits when fit instead of a power-law ($\chi^2/\text{DoF} = 342.1/231$). Similar results are obtained in the time-divided spectra. The results of these fits are summarised in Table 2. Assuming a metal abundance nine times the solar value and a plasma temperature of 4.1 keV (the best-fit values from Reeves et al. 2002a), an upper-limit to any thermal emission of $3.7 \times 10^{-14} \text{ erg cm}^{-2} \text{ s}^{-1}$ is determined, 11% of the total flux.

5. Discussion

The afterglow of GRB 020322 is the brightest observed to date by *XMM-Newton*, with $\sim 30\%$ more source counts than the detection of GRB 011211. It shows no evidence for line emission, permitting at most $\sim 10\%$ of the flux to come from a line-dominated thermal component similar to that observed in GRB 011211. This result contrasts with the detection of luminous emission lines and the good fit achieved with a thermal plasma model to the three previous detections of GRB afterglows with *XMM-Newton* (GRB 001025A, GRB 010220 and GRB 011211). It is worth noting that under similar time constraints (i.e. ~ 15 hours after the burst) significant thermal emission is not detectable in the afterglow spectrum of GRB 011211 either. It is possible therefore that thermal emission could have dominated the early-time spectrum of the afterglow of GRB 020322 *before* the time of this observation. The uncertainty surrounding the line-dominated component of the afterglow spectra (due to the few available results) also allows

Table 2. Goodness of fit in terms of χ^2 and numbers of degrees of freedom (χ^2/DoF) to a) the complete EPIC dataset, b) the first 11 ks of exposure and c) the remaining 15 ks of exposure, for six different models made up of three components: a power-law (PL), a redshifted neutral absorbing gas (Abs_z), and a collisionally-ionised plasma (VMEKAL). All models include absorption by the Galaxy ($4.6 \times 10^{20} \text{ cm}^{-2}$).

Model	PL	Abs _z +PL	PL+VMEKAL	Abs _z +PL+VMEKAL	VMEKAL	Abs _z +VMEKAL
Complete	437.4/234	241.5/232	364.4/230	239.1/229	398.6/232	342.1/231
0–11 ks	203.5/116	123.9/114	155.3/112	117.5/111	179.0/114	162.5/113
11–26 ks	189.0/123	109.4/121	151.6/119	108.4/118	161.6/121	138.6/120

us to speculate that the afterglow spectrum of GRB 020322 may have become line-dominated *after* the end of the *XMM-Newton* observation. The resolution of this question requires continuous monitoring of GRB X-ray afterglows for as long as two days after the burst. This may soon be possible using a combination of *Swift* (Gehrels 2000) and *XMM-Newton*.

It seems very likely that GRBs are highly collimated, relativistic events, with the beam angle constrained to less than $\sim 30^\circ$ (Frail et al. 2001, Panaitescu & Kumar 2001, Quilligan et al. 2002). Bursts observed with small viewing angles to the jet may have apparently brighter synchrotron afterglows. In this case, where the angle of the jet to the line of sight is small and a brighter afterglow is observed, isotropic line emission would be more difficult to detect.

A notable difference between this spectrum and that of GRB 011211 is the excess absorption required to fit the data in this case. It is possible that the absorbing gas is ionised. However, in either case the redshift must be high enough to shift the absorption edges out of the band (where the gas has metal abundances similar to or greater than the solar value, a reasonable assumption given that many GRBs are associated with strongly star-forming regions, e.g. Holland & Hjorth 1999).

Extrapolating the best-fit unabsorbed X-ray (synchrotron) power-law model into the optical R-band, gives an upper limit to the unreddened magnitude of 19.4 ± 0.6 (though this extrapolation may be further complicated by the presence of inverse Compton emission in the X-ray spectrum, see for example Harrison et al. 2001). The observation of Greiner et al. (2002) occurred during the *XMM-Newton* observation where they detect an optical transient with an R-band magnitude of 23.80 ± 0.30 . This implies an observed-frame extinction of, at most, $A_R = 4.4 \pm 0.9$, a degree of extinction at least concurrent with the fact that some GRBs are associated with regions of vigorous star-formation (see for example Holland & Hjorth 1999). This value is consistent with the detected X-ray column density at $z = 1.8$, assuming a Galactic gas-to-dust ratio.

The detection of a potential host galaxy with a magnitude of ~ 27 (Burud et al. 2002) is also consistent with the redshift range derived from the X-ray absorbing column, assuming a distribution of host galaxy magnitudes similar to either the Hubble Deep Field North (Cohen et al. 2000) or a sample of GRB host galaxies (Bloom et al. 2002a).

6. Conclusions

XMM-Newton detected the afterglow of GRB 020322 with a mean observed 0.2–10.0 keV flux of $3.5 \pm 0.2 \times$

$10^{-13} \text{ erg cm}^{-2} \text{ s}^{-1}$, making it the brightest X-ray afterglow observed with this satellite so far. Fitting a power-law to the lightcurve yields a best-fit decay index of 1.26 ± 0.23 . The spectrum – the best quality spectrum of a GRB X-ray afterglow to date – is well fit with a power-law absorbed with neutral or ionised gas significantly in excess of the Galactic column at redshift $1.8_{-1.1}^{+1.0}$ and/or with low metallicity. No emission features are detected in the spectrum and a thermal (mekal) model fits the data poorly, the upper limit on its contribution to the spectrum (assuming a 4 keV plasma with nine times the solar metal abundances) is $3.7 \times 10^{-14} \text{ erg cm}^{-2} \text{ s}^{-1}$ ($\sim 10\%$ of the total flux), indicating that if a thermal component was present in the early-time afterglow, it faded below a detectable level within the first ~ 15 hours, making it much fainter than the synchrotron emission.

Acknowledgements. This work is based on observations obtained with *XMM-Newton*, an ESA science mission with instruments and contributions directly funded by ESA Member States and the USA (NASA).

References

- Amati L., Frontera F., Vietri M. et al., 2000, *Sci* 290, 953
 Antonelli L. A., Piro L., Vietri M. et al., 2000, *ApJ* 545, L39
 Böttcher M., Dermer C. D., Crider A. W., Liang E. P., 1999, *A&A* 343, 111
 Bloom J. S., Kulkarni S. R., Djorgovski S. G., 2002a, *AJ* 123, 1111
 Bloom J. S., Mirabal N., Halpern J. P., Fox D. W., Lopes P. A. A., 2002b, GRB Coordinates Network Circular 1294
 Bloom J. S., Mirabal N., Halpern J. P., Fox D. W., Lopes P. A. A., 2002c, GRB Coordinates Network Circular 1296
 Burud I., Fruchter A., Rhoads J., Levan A., 2002, GRB Coordinates Network Circular 1536
 Cohen J. G., Hogg D. W., Blandford R. et al., 2000, *ApJ* 538, 29
 Dickey J. M., Lockman F. J., 1990, *ARA&A* 28, 215
 Ehle M., Rodriguez-Pascual P., Loiseau N. et al., 2002, GRB Coordinates Network Circular 1293
 Frail D. A., Kulkarni S. R., Sari R. et al., 2001, *ApJ* 562, L55
 Fynbo J. U., Jensen B. L., Gorosabel J. et al., 2001, *A&A* 369, 373
 Gandolfi G., 2002, GRB Coordinates Network Circular 1291
 Gehrels N., 2000, In: AIP Conf. Proc. 526: Gamma-ray Bursts, 5th Huntsville Symposium, p. 671
 Greiner J., Thiele U., Klose S., Castro-Tirado A. J., 2002, GRB Coordinates Network Circular 1298
 Harrison F. A., Yost S. A., Sari R. et al., 2001, *ApJ* 559, 123
 Holland S., Hjorth J., 1999, *A&A* 344, L67
 Jansen F., Lumb D., Altieri B. et al., 2001, *A&A* 365, L1
 Lazzati D., Ghisellini G., Amati L. et al., 2001, *ApJ* 556, 471
 Lazzati D., Perna R., 2002, *MNRAS* 330, 383
 Liedahl D. A., Osterheld A. L., Goldstein W. H., 1995, *ApJ* 438, L115
 McMillan R. J., Lamb D. Q., York D. G., 2002, GRB Coordinates Network Circular 1299

- Mewe R., Gronenschild E. H. B. M., van den Oord G. H. J., 1985, *A&AS* 62, 197
- Panaitescu A., Kumar P., 2001, *ApJ* 554, 667
- Piro L., 2001, In: E. Costa, F. Frontera, J. Hjorth (eds.), *Gamma-Ray Bursts in the Afterglow Era*, pp 97–103, Springer
- Piro L., 2002, *GRB Coordinates Network Circular* 1290
- Piro L., Amati L., Antonelli L. A. et al., 1998, *A&A* 331, L41
- Piro L., Garmire G., Garcia M. et al., 2000, *Sci* 290, 955
- Quilligan F., McBreen B., Hanlon L. et al., 2002, *A&A* 385, 377
- Reeves J. N., Watson D., Osborne J. P., Pounds K. A., Brien P. T. O., 2002a, *astro-ph/0206480*
- Reeves J. N., Watson D., Osborne J. P. et al., 2002b, *Nat* 416, 512
- Strüder L., Briel U., Dennerl K. et al., 2001, *A&A* 365, L18
- Tedds J. A., Watson M. G., 2002, In: F. Jansen (ed.), *New Visions of the X-Ray Universe in the XMM-Newton and Chandra Era*, ESA SP-488
- Turner M. J. L., Abbey A., Arnaud M. et al., 2001, *A&A* 365, L27
- Vietri M., Stella L., 1998, *ApJ* 507, L45
- Watson D., Reeves J. N., Osborne J. et al., 2002, *A&A* 393, L1
- Woosley S. E., 1993, *ApJ* 405, 273
- Yoshida A., Namiki M., Yonetoku D. et al., 2001, *ApJ* 557, L27